Developing an algorithm for local anomaly detection based on spectral space window in hyperspectral image

Article *in* Earth Science Informatics · January 2015

DOI: 10.1007/s12145-014-0200-4

4 authors, including:

Jonathan Li
University of Waterloo
252 PUBLICATIONS **3,240** CITATIONS
SEE PROFILE

Saied Pirasteh
University of Waterloo
106 PUBLICATIONS **857** CITATIONS
SEE PROFILE

Earth Sci Inform
DOI 10.1007/s12145-014-0200-4

RESEARCH ARTICLE

Developing an algorithm for local anomaly detection based on spectral space window in hyperspectral image

Zhiyong Li · Jonathan Li · Shilin Zhou · Saied Pirasteh

Received: 18 August 2014 / Accepted: 12 December 2014

Abstract A local anomaly detection algorithm based on sliding windows in spectral space has been proposed in this research. The traditional local anomaly detection algorithms are implemented in spatial windows because local data of an image scene is more suitable for a single statistical model than global data. However, from the aspect of geometric structure of a dataset, this assumption is not entirely proper. As multivariate data, the hyperspectral image dataset can be considered as a low-dimensional manifold, embedded in the high-dimensional spectral space. The nonlinear spectral mixture occurs more frequently, as well as a low dimensional manifold being nonlinear. The traditional spatial local anomaly detection algorithms based on linear projection would not be appropriate to deal with this kind of data. This paper studies the local linear ideas in manifold learning, and an anomaly detection algorithm has been implemented based on the linear projections in a local area of spectral space. The key concept is that a small neighborhood areas of nonlinear manifold can be considered as a local linear structure. The classic spatial local algorithms and proposed algorithm are compared by using real hyperspectral images from vehicle and aviation platforms. The results demonstrated the effectiveness of the proposed algorithm in improving detection of the weak anomalies that decreases the number of false alarms.

Keywords Remote sensing · Hyperspctral · Local anomaly detection · Nonlinear manifold

Communicated by: H. A. Babaie

Z. Li (✉) · S. Zhou
School of Electronic Science and Engineering, National University of Defense Technology, Changsha, Hunan 410073, China
e-mail: lzylmz75@gmail.com

J. Li
School of Information Science and Engineering, Xiamen University, Xiamen, Fujian 361005, China

Z. Li · J. Li · S. Pirasteh
Department of Geography & Environmental Management, Faculty of Environment, University of Waterloo, Waterloo, ON N2L 3G1, Canada

Background and introduction

Anomaly detection is nowadays a very active research topic for automated analysis of hyperspectral imagery. Without prior spectral information and atmospheric correction, anomaly detectors can identify the pixels that are different in spectrum from the background (Stein et al. 2002; Huck and Guillaume 2010).

Historically, algorithms to target and anomaly detection in hyperspectral imagery could be divided into two categories based on different data models (Ahlberg et al. 2004), as a) detectors based on unstructured models and b) detectors based on structured models. The unstructured models referred to no specific geometric structure on the data. They were also called probabilistic, statistical, and/or data-driven. Anomaly detection methods based on unstructured models were traditional and familiar. They encompassed the well-known RX detector (Reed and Yu 1990) and its improvement, (i.e. SSRX detector) (Schaum 2007; Borghys et al. 2012). Detectors using structured models are based on linear subspace or Linear Mixture Model (LMM), such as Orthogonal Subspaces Projection (OSP) that is developed by Harsanyi et al. (1994)), and Low Probability Detection (LPD) (Harsanyi et al. 1994; Chang 2005). It is interesting that both structured and unstructured detectors have performed the same functional form of matched filter or linear projection (Chang and Chiang 2002).

Published online: 08 January 2015

In general, the anomaly detection algorithms can be implemented either in global or local area of an image scene. There were 2 ways to carry out the local detectors (Bachega et al. 2011), a) sliding spatial windows and b) segmentation of an image scene. The key concept of both methods was that local data of an image scene was more suitable for a single statistical model. RX algorithm was derived from hypothesis tests based on multivariate Gaussian distribution. It was always considered as a local method, such as Local RX and Qausi Local RX (Borghys et al. 2012).

However, as nonlinear spectral mixture frequently occurs in the real environment, the nonlinear manifolds would be more common. In this case, anomaly detection based on linear projection could not deal with these data efficiently. Thus, there were many kernel based detectors, such as kernel RX and kernel OSP (Nasrabadi 2014). They handled this problem by using the kernel functions to implement linear projections in high dimensional feature space. Another two kinds of detectors were developed to treat this problem. One was to use the local topological structure to calculate the Weighted Vertex Volume (Messinger and Chester 2011) and extract the "outliers" in the local spatial image. Basically, outlier detection is aimed at discovering anomalous or inconsistent patterns from a dataset. This was one of the major tasks in data mining when working on a large dataset (Zhao and Saligrama 2009; Ramaswamy et al. 2000). Similar research has also shown in the literatures of Du and Zhang (2014a, 2014b). The patches with a locally linear structure were used to fit the manifold structure of the entire hyperspectral image. The other kind of detectors focused on manifold embedding methods (Li et al. 2010a, 2010b). Agovic et al. (2007) had studied anomaly detection in transportation corridors using manifold embedding. They investigated the usefulness of manifold embedding methods for feature representation in anomaly detection problems. The study was focused on both linear methods, such as multi-dimensional scaling (MDS), as well as nonlinear methods, such as locally linear embedding (LLE) and isometric feature mapping (ISOMAP).

The traditional detectors based on linear projection could not extract the weak anomaly points from the nonlinear spectra mixture dataset because the prominence of anomalies would be reduced after linear projection. If these detectors are implemented in a small area of data manifold, then their local structures can be linear and the detectors based on linear projection would become effective. This is the motivation of the proposed algorithm in this paper. By using the concept of local linearity from manifold learning methods (Seung and Lee 2000), the sliding windows were established in spectral space and the local data would be considered as a linear manifold. Thus, the detector based on linear projections was implemented in spectral space windows. The Low Probability Anomaly Detection (LPAD) detector (Li et al. 2014) would be implemented on these sliding windows of spectral space. This algorithm is called LPAD based on Spectral Space Window (SSW-LPAD). In Section II, the relationship between nonlinear manifolds of datasets and anomalies are introduced; Section III is the methodology of the algorithm based on spectral space window; Section IV is description of image data; Section V is the results analysis and the comparative analysis between this algorithm and spatial local algorithms.

Nonlinear manifold and anomalies

As a kind of multivariate data, hyperspectral image may be considered to be a low dimensional manifold in spectral space. Usually, the dimension of this manifold is called intrinsic dimension (Verveer, Peter j., Robert P. W. Duin 1995). If the datasets fit description of the Linear Mixed Model (LMM), the manifold can be a linear and also may be regarded as a hyper-plane or a linear hyper-simplex (Koppen 2000). In this case, the entire datasets can be linearly projected into a subspace. The dimension of this subspace is the intrinsic dimension of the whole datasets. The dispersion of the original data can be represented accurately by this linear subspace.

On the other hand, the lower dimensional manifold would be nonlinear if the datasets fit the description of the non-linear mixed model, such as a hyper-curved surface or a nonlinear hyper-simplex (Koppen 2000). The geometric structure of nonlinear manifolds is particular. The dataset cannot be represented accurately by utilizing the linear transformations (i.e. translation, rotation and scaling) in the intrinsic dimensional subspace. A higher dimensional linear subspace should be used to contain it.

For anomaly detection, nonlinear properties of the manifold have considerable effects on the detectors based on linear projections. An example in a low dimensional space (3D) can illustrate this problem. Figure 1a shows a 2D curve and one anomaly point in 3D space and Fig. 1b shows a 2D curved-surface and one anomaly point in 3D space. The curve C (in Fig. 1a) is considered as a nonlinear manifold and its intrinsic dimension is 1. Pt is an anomaly point. The points of the curve C and anomaly point Pt are all located on the plane P. It is obvious that point Pt will be submerged into the points of curve C by using the detectors based on linear orthogonal projections, because the curve was the main part of this dataset. Thus, in order to suppress the points of the curve effectively, the detectors based on linear orthogonal projections will project all points to the orthogonal space of plane P in 3D space. However, point Pt belongs to the plane P, so it will be suppressed like points of curve C. It is hard to distinguish Pt from the projected image. The case of Fig. 1b has the same problem.

However, if the nonlinear manifold data has been handled by detectors based on linear projections, some weak anomaly points which were close but did not belong to the background

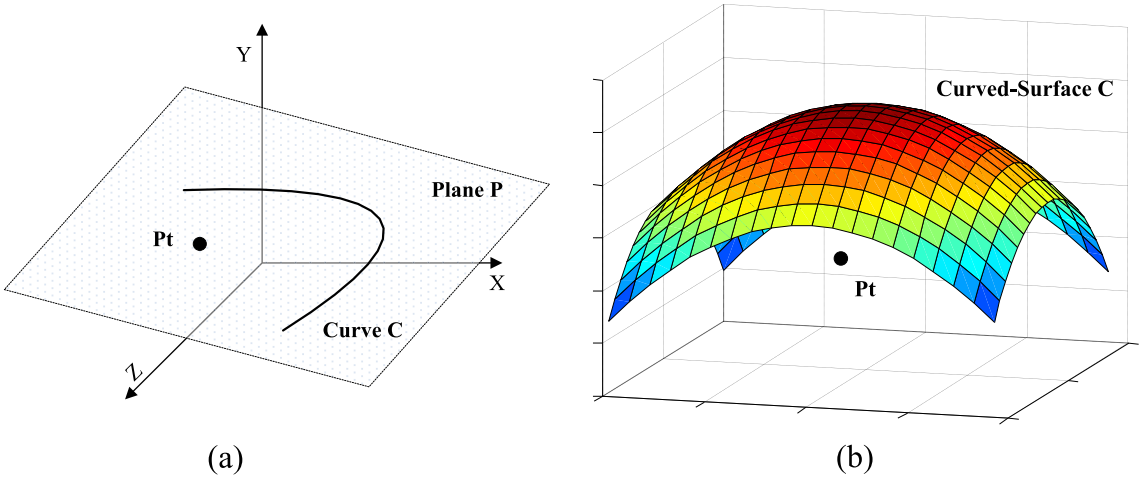

Fig. 1 Nonlinear manifold and anomaly point. **a** 2D curve and anomaly point; **b** 3D curve surface and anomaly point

nonlinear manifold would be ignored, even for local data of an image scene. Therefore, if a small area is segmented from this manifold, it would be considered as a linear structure and the weak anomaly points could be distinguished effectively by using the detectors based on linear projections. This is the main motivation of the proposed method.

Method

It is important to compare the performance between the proposed algorithm and algorithms based on spatial window. Here, the Local RX(LRX) and Local OSP(LOSP) (Chao et al. 2009) algorithms will be considered. In this section, the LRX and LOSP are introduced first, and the SSW-LPAD algorithm has been discussed.

Local RX (LRX)

The RX algorithm is a constant false alarm rate (CFAR) adaptive anomaly detector that is derived from the generalized likelihood ratio test (GLRT). It was considered as the benchmark anomaly detection algorithm for hyperspectral data (Messinger and Chester 2011). RX algorithm is based on the assumption that the background statistics could be modeled as a multivariate Gaussian distribution:

$$D_{\mathrm{RXD}}(\boldsymbol{x_i}) = (\boldsymbol{x_i}-\boldsymbol{\mu})^T\mathbf{C}^{-1}(\boldsymbol{x_i}-\boldsymbol{\mu})\begin{cases}\geq\eta, & \textit{anomaly present}\\ <\eta, & \textit{anomaly absent}\end{cases} \tag{1}$$

Where $\boldsymbol{\mu}=\frac{1}{N}\sum_{i=1}^{N}\boldsymbol{x_i}$ is the mean spectrum, $\mathbf{C}=\frac{1}{N}\sum_{i=1}^{N}(\mathrm{x_i}-\boldsymbol{\mu})(\mathrm{x_i}-\boldsymbol{\mu})^T$ is covariance matrix. $\boldsymbol{x_i}$ are the pixel spectra of image data, subscripts $\boldsymbol{i}$ refer to the i^{th} pixel spectrum in the image dataset.

Usually, RX algorithm is regarded as a local detector, but it can handle global data as well. In the implementation of LRX, the covariance matrix and the mean spectrum of the background were estimated locally in a window around the pixel under test (PUT). A double sliding window was used: a guard window and the outer window were defined, and the background statistics were determined using the pixels between them. See Fig. 2.

Local orthogonal subspaces projection (LOSP)

LOSP algorithm (Chao et al. 2009) is based on the assumption that the variation of terrain is small in the local area of an image scene. In other word, the mean spectrum presents the background, and it uses constructing orthogonal projected operators. If the spectrum of PUT is $\boldsymbol{d}$ and the mean spectrum of the sliding window is $\overline{d}$ then the detector of LOSP will be:

$$P_{\mathrm{LOSP}} = \kappa\boldsymbol{d}^T\left[\mathbf{I}-\overline{\boldsymbol{d}}\left(\overline{\boldsymbol{d}}^T\overline{\boldsymbol{d}}\right)^{-1}\overline{\boldsymbol{d}}^T\right] \tag{2}$$

Where $\overline{\boldsymbol{d}}=\sum_{i=1}^{m}\boldsymbol{y}_i$, $\boldsymbol{y_i}$ are the spectra except PUT in the window. κ is a constant for normalization.

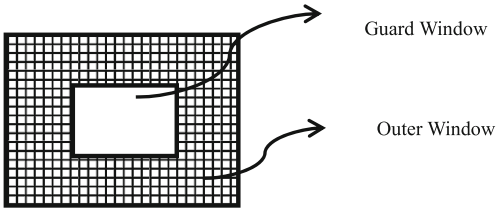

Fig. 2 Double spatial windows of LRX

Spectral space window LPAD (SSW-LPAD)

In SSW-LPAD, LPAD algorithm has implemented sliding windows in spectral space. LPAD algorithm has been derived upon data linear manifold assumption (Li et al. 2014). In this algorithm, the entire image dataset is modeled as a linear manifold. Although, it does not fit the real situation, the linear manifold is a simple and feasible assumption to the hyperspectral dataset. If an image dataset is considered as a linear manifold, anomalies would not located in this manifold because of the spectral independence. The distances along the particular vertical direction could be used to evaluate whether the points are anomalies or background. The purpose of LPAD is to find these special directions.

The vertical subspace can be derived from linear equations. Firstly, the general plane equation in 3-D Euclidean space is considered and extended to describe the linear manifold in high dimensional space. Suppose that there is a dataset D_a which distributes in a linear manifold in l -dimensions space, all of the vectors $\boldsymbol{\alpha}=(a_1,a_2,\cdots a_l)$ in dataset D_a fit the following equation:

$$x_1a_1 + x_2a_2 + \cdots + x_la_l + x_{l+1} = 0 \tag{3}$$

Where, the non-zero vector $\boldsymbol{X} = (x_1 \quad x_2 \quad \cdots \quad x_{l+1})$ is the normal vector of this linear manifold. With respect to linear algebra, equation (3) means all the vectors α of D_a can linearly express each other. After removing the mean vector of dataset, the matrix form of equation (3) could be rewritten as:

$$AX = 0 \tag{4}$$

A is a $N\times l$ matrix. The row vectors in **A** represents a l -dimension vector of the dataset. N is the number of samples in the dataset. $\boldsymbol{X}$ is the l -dimensional column vector which represents the normal vector.

Considering the hyperspectral image dataset, the main parts of geometrical structure would be composed of background data and would be a linear manifold. The anomalies would be located outside of the manifold. Therefore, the anomalies could be distinguished from the manifold efficiently if the proper decision boundary along the normal direction could be found. In fact, Equation (4) is a homogeneous linear equation. In this case, the extraction of normal vectors is converted to solving the homogeneous linear equations. The matrix **A** is a singular matrix because the row vectors has denoted as a linear combination of the others. Therefore, the solution of the equation (4) would not be unique, and it has a solution set. We used the Moore–Penrose pseudoinverse (Barata and Hussein 2012) to calculate it. If some rows of **A** are linearly independent, the solution set (in terms of least squares) of equation (4) could be derived from the Moore–Penrose pseudoinverse:

$$\boldsymbol{x}_0 = (\mathbf{E}-\mathbf{U}^+\mathbf{U})\boldsymbol{\xi} \tag{5}$$

$\mathbf{U}^+$ denoted Moore–Penrose pseudoinverse, where $\mathbf{U}^+=\mathbf{U}^T(\mathbf{U}\mathbf{U}^T)^{-1}$. **U** is $k\times l$ matrix, it is constructed by k independent rows of **A.** **E** is the identity matrix and $\boldsymbol{\xi}$ is an arbitrary l -dimension vector.

Because $\boldsymbol{\xi}$ is an arbitrary l -dimension vector, we could use the spectrum of PUT to replace it. Thus, the vertical distance (along the normal direction of manifold) between the PUT and background manifold can be calculated as:

$$D(\boldsymbol{\alpha}) = \boldsymbol{\alpha}^T(\mathbf{E}-\mathbf{U}^+\mathbf{U})\boldsymbol{\alpha} = \boldsymbol{\alpha}^T\left(\mathbf{E}-\mathbf{U}^T\left(\mathbf{U}\mathbf{U}^T\right)^{-1}\mathbf{U}\right)\boldsymbol{\alpha} \tag{6}$$

Where, $\boldsymbol{\alpha}$ represents the spectrum of PUT. The key of these calculations is matrix **U**. Usually, **U** is composed of the endmembers of background. However, for the convenient calculation, the larger eigenvectors have been used to replace the background endmembers. Thus, the equation became:

$$D(\boldsymbol{\alpha}) = \boldsymbol{\alpha}^T(\mathbf{E}-\mathbf{V}^+\mathbf{V})\boldsymbol{\alpha} = \boldsymbol{\alpha}^T\left(\mathbf{E}-\mathbf{V}^T\left(\mathbf{V}\mathbf{V}^T\right)^{-1}\mathbf{V}\right)\boldsymbol{\alpha} \tag{7}$$

Where, **V** is composed of the magnificent eigenvectors of the data covariance matrix. This detector is called Low Probability Anomaly Detection (LPAD) because it is similar to the LPD detector (Chang 2005). The significant difference is the unit vector in LPD that is replaced by the spectrum of PUT in LPAD.

In this paper, we implemented the LPAD on the sliding windows in spectral space. By calculating the Euclidean distance between two arbitrary points of spectral pixels, a list of nearest neighbors has been established for each PUT. Alternatively, double sliding windows have defined to be a guard window and the outer window. The size of the outer window is defined as K nearest neighbors, and the size of the guard window is defined as G nearest neighbors. The spectrums between the two windows are used to calculate matrix **V**. It is worth noting that the radii of these windows are variable because the density is different throughout the whole manifold. Theoretically, taking into account the requirements of the minimum number of pixels for the detection algorithm, the entire pixels between the two windows should form a linear manifold. Similarly, for the areas with different in density, the numbers of K and G should be mutative. However, its computation and complexity is very high, therefore, a constant

Table 1 Main parameters of two spectrometers

Name of Spectrometer Parameter	FISS	OMIS
Spectral coverage (μm)	0.4–0.9	0.4 - 12.5
Spectral resolution (nm)	1.4	10–500
Number of band	344	128
IFOV (mrad)	1	3–5
Height of sensor (m)	30	1000

number has been chosen for convenience of calculation in this paper.

Data collection and description

To assess the performance and compare the effectiveness of different algorithms, two groups of hyperspectral data were used in experiments. One was from Field Imaging Spectrometer System (FISS) and the other was from Operative Modular Imaging Spectrometer (OMIS), which was produced by the Shanghai Institute of Technical Physics (SITP) of the Chinese Academy of Sciences. The basic parameters of the two imaging spectrometers have been shown in Table 1.

The data of FISS was collected by the vehicle platform and placed 30 m from the ground. The size of the image to be processed was 230×230 pixels and 86 bands has been selected. The anomalies in FISS data were small planks. They depicted in green color and put in a corn field (see Fig. 3). Fig. 3a is a hyperspectral image cube and Fig. 3b is the digital pictures. There are 15 pieces of planks, and their spatial sizes are about 6–10 cm. In Fig. 3b, the white dots indicate the actual position of these planks.

The data of OMIS was achieved by the actual flight of the airborne platform. Image size is 250×250 pixels. Because of the low SNR, the bands of vapor absorption are removed, and only 80 bands have been processed in this research. The Original image and ground truth data have shown in Fig. 4. The anomalies have two parts. One is the vehicles in the center of the image (i.e. labeled from T1 to T7 in Fig. 4b), and the other is 8 white tiles at the top of the image.

Results and discussion

Four algorithms have been compared by utilizing the two hyperspectral images. They are global LPAD, LRX, LOSP and SSW-LPAD. The size of the outer window is set as 15×15 pixels and the guard window is 5×5 pixels. The number of magnificent eigenvectors was nine for FISS data and six for OMIS data. Figure 5 is the projected image of four algorithms for FISS data. Figure 6 is the projected image of four algorithms for OMIS data.

The thresholds are calculated by exploiting the Constant False Alarm Rate (CFAR) algorithm in the projected images. Here, we utilized the CFAR based on the lognormal distribution. The experimental ROC curves (Matteoli et al. 2010) have been calculated and used to assess the performance. The ex-ROC curves are derived from counting the number of targets correctly detected, and the corresponding number of false alarms (see Fig. 7). Fig. 7 is the ex-ROC curves of the four detectors for FISS and OMIS data.

The influence of the two parameters (K and G) on the detection performances show in Fig. 8. The SSW-LPAD algorithm and OMIS dataset are used here. Usually, guard window G are determined by the targets, spatial size and image resolution.

Firstly, on the basis of the fixed K, the experimental ROC curves on different G are calculated, such as Fig. 8a. Obviously, G should not be too big. At the same time, it should not be too small. Because of the mixture of spectra, there would be

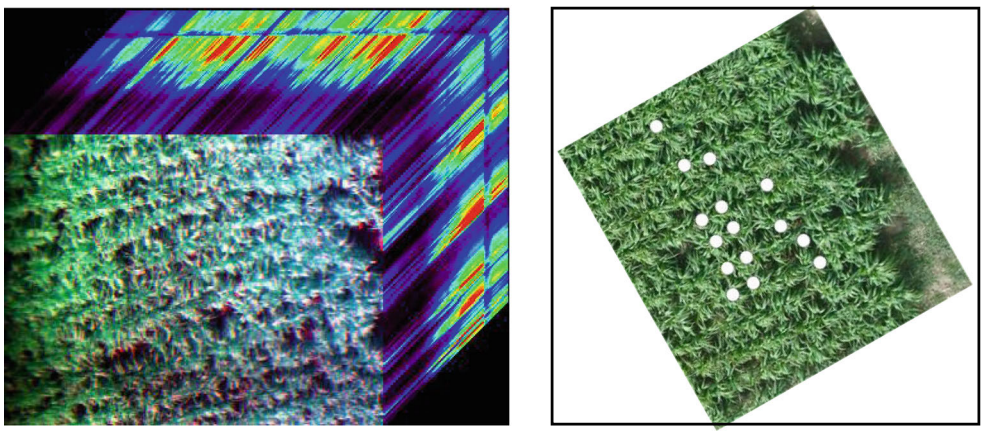

(a) (b)

Fig. 3 FISS data cube and targets position. **a** Data cube; **b** Digital photo

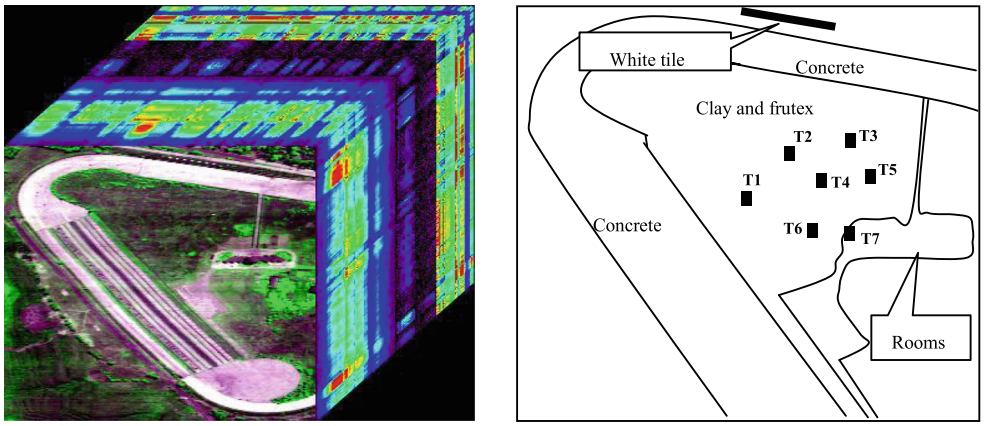

Fig. 4 OMIS data cube and the anomalies position. **a** Data cube; **b** Anomalies position

many pixels that have a similar spectrum as the targets in image. If G is small, these pixels may involve in the orthogonal projection and the separation between targets and background will be decreased.

On the other hand, the experimental ROC curves on different K are calculated based on the fixed G, such as Fig. 8b. Different K were tested, and only six curves were shown here. For the first few easily detected anomalies, the six curves were similar. However, for the last few weak anomalies, the performances of detectors with K greater than 200 were much better. It meant that outer windows should be big enough to form the local linear manifolds (at least 5~6 times more than the G).

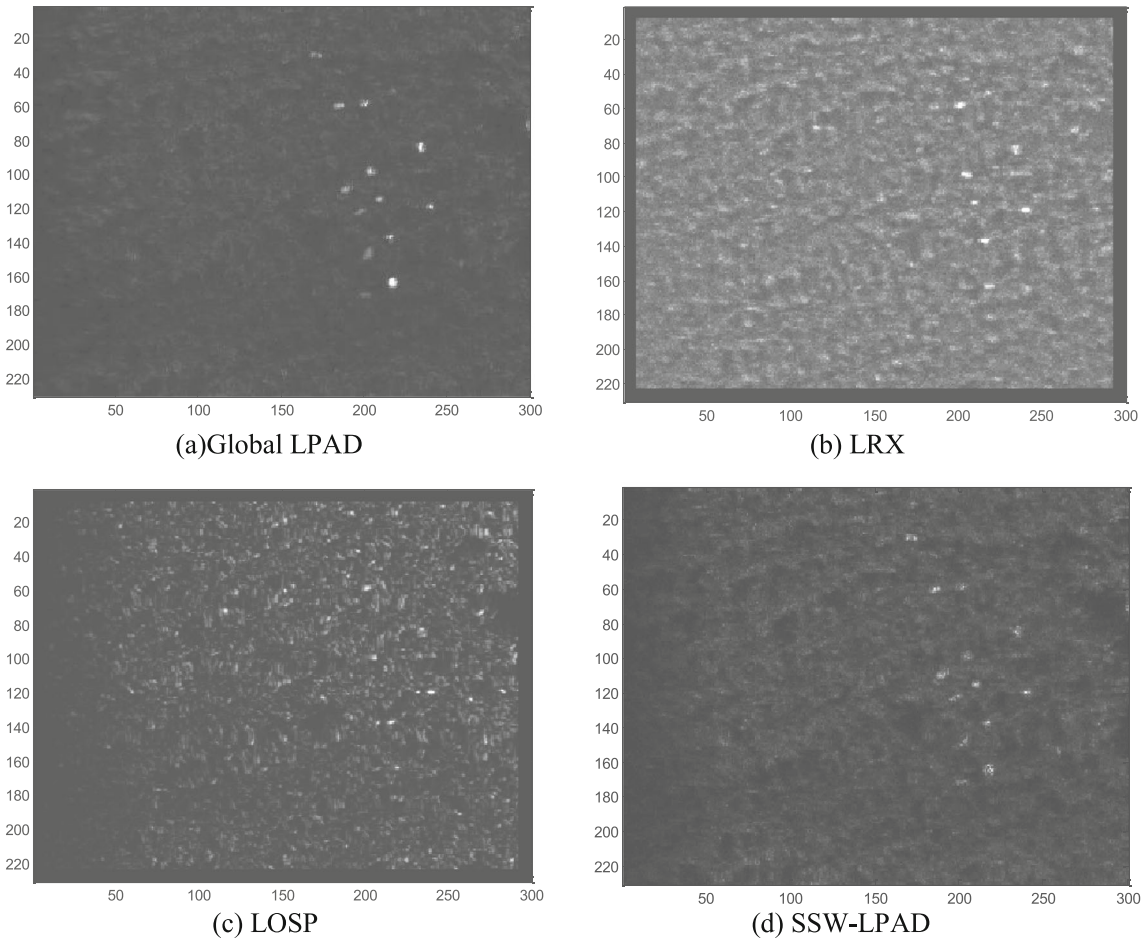

Fig. 5 FISS data projected images of four algorithms. **a** Global LPAD; **b** LRX; **c** LOSP; **d** SSW-LPAD

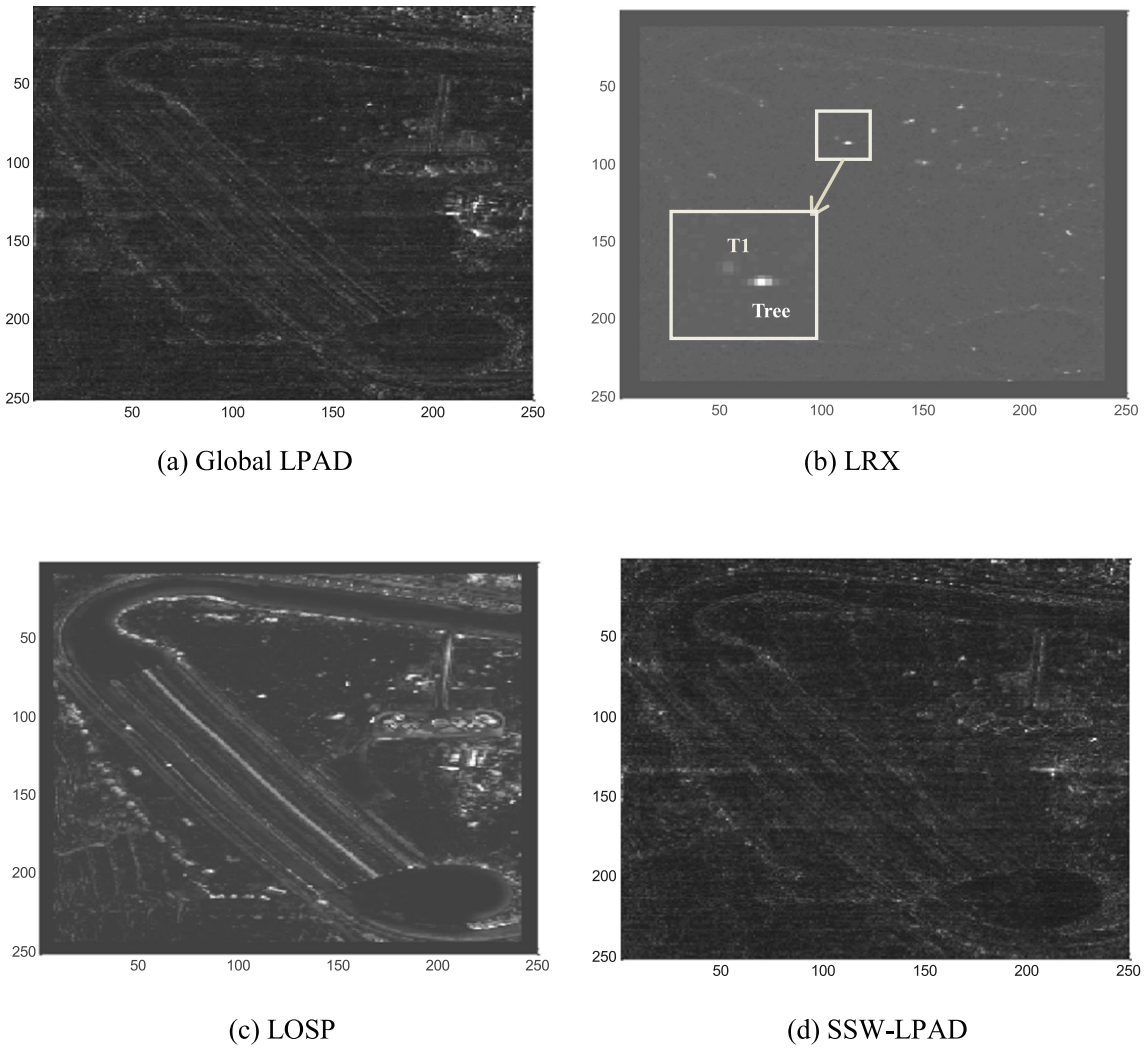

Fig. 6 OMIS data projected images of four algorithms. **a** Global LPAD; **b** LRX; **c** LOSP; **d** SSW-LPAD

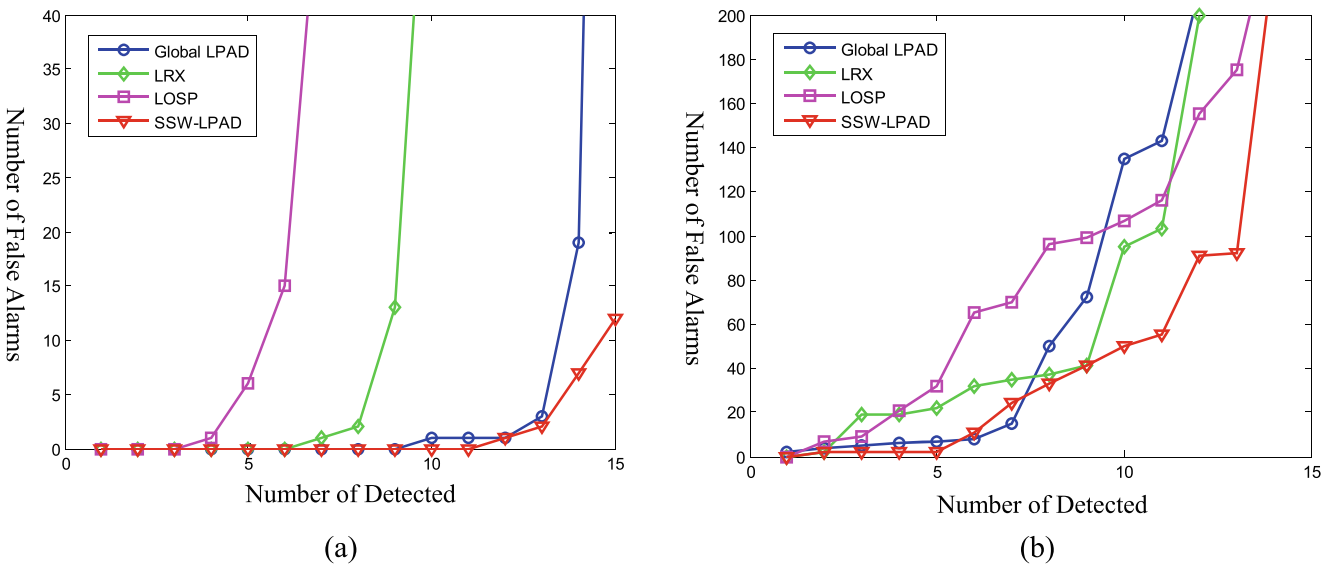

Fig. 7 Experimental ROC curves of four algorithms of FISS and OMIS data. **a** Experimental ROC curves of FISS data; **b** Experimental ROC curves of OMIS data

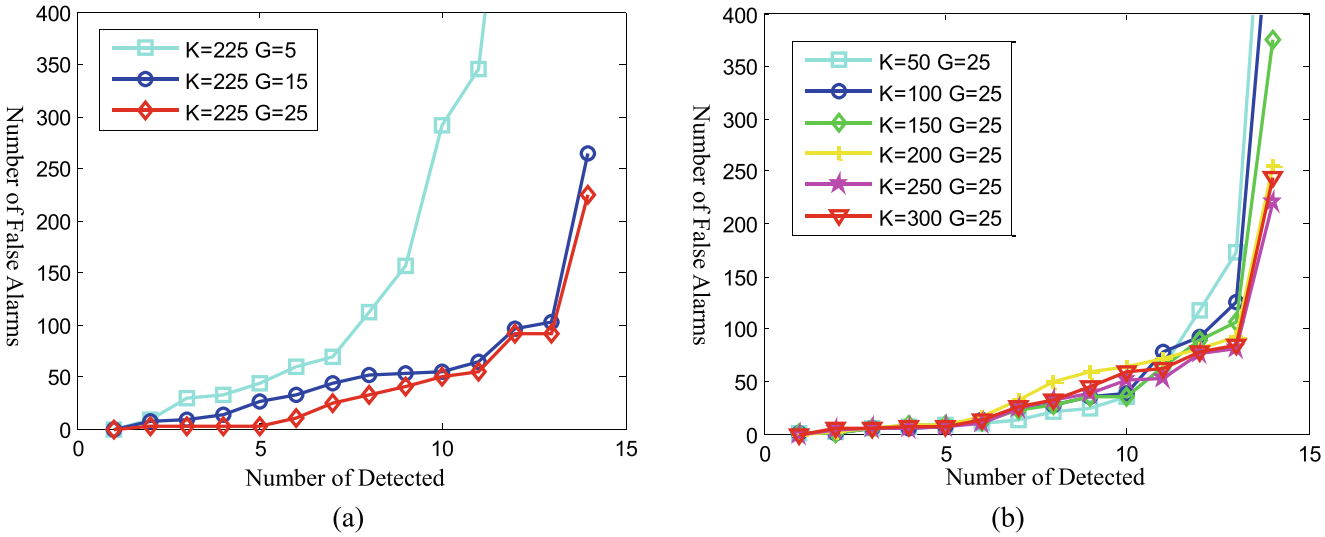

Fig. 8 Experimental ROC curves of SSW-LPAD algorithms and OMIS dataset based on different K and G. **a** Experimental ROC curves of different G; **b** Experimental ROC curves of different K

Small K would lead to a decrease in detection performance. Alternatively, the bigger value of K was not necessary. In Fig. 8b, the detection performances of detectors with K greater than 200 were similar.

The experiments and analyses of this study have revealed that

1) Overall, SSW-LPAD outperformed the global and spatial local detectors, especially in background suppression (see Figs. 5d and 6d). The texture of SSW-LPAD background has almost disappeared in the projected image. In the case of the same targets in the detection, SSW-LPAD algorithm has a lower number of false alarms. See Fig. 7.
2) Among the structured model based detectors, SSW-LPAD outperformed global LPAD and LOSP, especially for FISS data. All targets have detected in case of the few false alarms (see Fig. 7a). In these algorithms, LOSP showed unsatisfactory results (see Figs. 5c and 6c). The main reason is that of using the mean spectrum was not enough to suppress energy of the background. According to the properties of the manifolds, local spatial data might not necessarily coincide with the one-dimensional linear manifold because of the complexity of the terrain. Therefore, LOSP would achieve the better results if more endmembers of background data could be used in the projections.
3) Although performances of SSW-LPAD were better than spatial local detectors, it was more outstanding in the projected image than others for particular targets (see target T1 in Fig. 6c). This case meant that LRX can distinguish the targets whose spectra were similar to the spectral neighbors, but different from the spatial neighbors. That also meant, for SSW-LPAD algorithm, an inappropriate neighborhood of local manifold might lead to failure of detection.

In summary, there were overall better performances for the local detectors based on spectral space window. This case showed that it was to be a reasonable and an effective approach to handling the nonlinear manifold by using the detectors based on spectral space window. It would improve the detection of weak anomalies and decrease the false alarms. However, there is a critical limitation that we encountered. The computational efficiency of SSW-LPAD was low. The calculation of the nearest neighborhoods list would be very time consuming when the image size is big. This paper recommends a motivating future research in finding a proper way to eliminate the aforementioned limitation and speed up the calculation.

Conclusion

Algorithms of SSW-LPAD have been derived from the geometric structure feature of low dimensional manifolds. By applying local linear concepts in nonlinear manifold, we established the sliding windows for neighborhood data in spectral space and implemented detectors based on linear projection in these local areas. Thus, the problem of global nonlinear data processing was converted into local linear ways; it improved the performance of detection. The experimental results and comparative analysis based on real hyperspectral image data demonstrated the effectiveness of the proposed algorithm. At the same time, it also validated the improvement of the local linear concept when dealing with the nonlinear manifold data in anomaly detection.

Acknowledgments This study was supported by the National Natural Science Foundation of China under the Grant 40901216.

References

Agovic, A., A. Banerjee, A. Ganguly, V. Protopopescu, 2007, Anomaly Detection in Transportation Corridors using Manifold Embedding, San Jose, CA. http://www-users.cs.umn.edu/~aagovic/kdd-anomaly2.pdf

Ahlberg J, Renhorn I, Forskningsinstitut T (2004) Multi-and Hyperspectral Target and Anomaly Detection. Linköping, FOI, Sweden

Bachega, L.R., J. Theiler, C.A. Bouman, 2011, Evaluating and improving local hyperspectral anomaly detectors, Applied Imagery Pattern Recognition Workshop (AIPR), doi: 10.1109/AIPR.2011.6176369 IEEE, pp1-8

Barata J. C. A., Hussein M. S., 2012, The Moore–Penrose pseudoinverse: A tutorial review of the theory, Brazilian Journal of Physics, (42): 146–165, doi: 10.1007/s13538-011-0052-z

Borghys, D., I. Kasen, V. Achard, C. Perneel, 2012, Comparative evaluation of hyperspectral anomaly detectors in different types of background. Proc. SPIE 8390, Algorithms and Technologies for Multispectral, Hyperspectral, and Ultraspectral Imagery XVIII

Chang CI (2005) Orthogonal subspace projection (OSP) revisited: a comprehensive study and analysis. IEEE Trans Geosci Remote Sens 43(3):502–518

Chang CI, Chiang SS (2002) Anomaly detection and classification for hyperspectral imagery. IEEE Trans Geosci Remote Sens 40(6): 1314–1325

Chao D, Huijie Z, Wei W (2009) Hyperpectral image anomaly detection based on local orthogonal subspace projection. Opt Precis Eng 17(8):2004–2010

Du B, Zhang L (2014a) A discriminative metric learning based anomaly detection method. IEEE Trans Geosci Remote Sens 52(11):6844–6857

Du B, Zhang L (2014b) Target detection based on a dynamic subspace. Pattern Recogn 47(1):344–358

Harsanyi, J. C., W. Farrand, and C.-I. Chang, 1994, Detection of subpixel signatures in hyperspectral image sequences. in Proc. Amer. Soc. Photogram. Remote Sens., Reno, NV, pp236-247

Huck A, Guillaume M (2010) Asymptotically CFAR-unsupervised target detection and discrimination in hyperspectral images with anomalous-component pursuit. IEEE Trans Geosci Remote Sens 48(11):3980–3991

Koppen, M., 2000, The curse of dimensionality, 5th Online World Conference on Soft Computing in Industrial Applications (WSC5), http://yaroslavvb.com/papers/koppen-curse.pdf

Li M, Crawford MM, Tian J (2010a) Anomaly detection for hyperspectral images based on robust locally linear embedding. Journal of Infrared, Millimeter, and Terahertz Waves 31(6): 753–762

Li M., Crawford M M, Tian J, 2010b, Anomaly detection for hyperspectral images using local tangent space alignment, Geoscience and Remote Sensing Symposium (IGARSS), 2010 I.E. International, pp824-827

Li ZY, Wang LL, Zheng SY (2014) Applied low dimension linear manifold in hyperspectral imagery anomaly detection, Proc. SPIE 9142:91421–91429

Matteoli S, Diani M, Corsini G (2010) A tutorial overview of anomaly detection in hyperspectral images. IEEE A&E Systems Magazine 25(7):5–27

Messinger DW, Chester F (2011) A graph theoretic approach to anomaly detection in hyperspectral imagery, 3rd hyperspectral image and signal processing: evolution in remote sensing (WHISPERS). Lisbon, pp 1–4

Nasrabadi NM (2014) Hyperspectral target detection-an overview of current and future challenges. IEEE Signal Processing Magzine, pp 34–44

Ramaswamy S, Rastogi R, Shim K (2000) Efficient algorithms for mining outliers from large data sets, SIGMOD '00 Proceedings of the 2000 ACM SIGMOD international conference on Management of data, pp 427–438

Reed IS, Yu X (1990) Adaptive multiple-band CFAR detection of an optical pattern with unknown spectral distribution. IEEE Transactions on Acoustics Speech and Signal Processing 38(10): 1760–1770

Schaum, A., 2007, Hyperspectral anomaly detection: Beyond RX. Proc. SPIE6565 Algorithms and Technologies for Multispectral, Hyperspectral and Ultraspectral Imagery XII, Paper on 656502

Seung H, Lee D (2000) The manifold ways of perception. Science 290(5500):2268–2269

Stein DWJ, Beaven SG, Lawrence Hoff E (2002) Anomaly detection from hyperspectral imagery. IEEE Signal Process Mag 19(1):58–69

Verveer, Peter j., Robert P. W. Duin, 1995, An Evaluation of Intrinsic Dimensionality Estimators, IEEE Trans. On Pattern Analysis and Machine Intelligence,Vol.17, NO.1, pp81-85

Zhao, M., V. Saligrama, 2009, Anomaly Detection with Score functions based on Nearest Neighbor Graphs, arXiv.org>cs>arXiv: 0910.5461v1